QUANTUM CONFINEMENT MODELING AND SIMULATION FOR QUANTUM WELL SOLAR CELLS

Laurenţiu FARA[1], Vladimir IANCU[1], Mihai Răzvan MITROI[1]

Abstract. *The present paper discusses the modeling of the multi-layered quantum well solar cells as well as the simulated results of this model. The quantum confinement of a semiconductor induces new energy levels, located in the band gap, as well as resonant levels located in the conduction and valence bands. These levels allow supplementary absorption in visible and near infrared range. The quantum efficiency of the supplementary absorption was calculated within the infinite rectangular quantum well approximation. As the absorption excites carriers in the gap of each layer, even a small absorption significantly increases the photocurrent (by photoassisted tunneling) and therefore the cell efficiency. There are presented the results of the simulation for Einstein absorption coefficient and quantum efficiency of the transition between the resonant levels of GaAs, as well as quantum efficiency of the transitions between the confinement levels.*

Keywords: Solar cell; Quantum Confinement Effects; Multi-layered structure; Optical Absorption; Quantum Well

1. Introduction

The "quantum well" photovoltaic cells were first proposed in 1990 [1], based on the idea that the use of the quantum wells could improve the photovoltaic cells by extending their spectral response, as well as by increasing the photocurrent. One year later, this idea was experimentally proved by using a $GaAs/Al_xGa_{1-x}As$ multi-layered structure [2]. From then on, the use of the multi-layered photovoltaic (MLPV) cells became one of the most used approaches for a high efficiency PV cell. Generally, such cells are p-i-n type diodes, with the intrinsic region formed by a multilayered structure [3-15]. Most of these cells have layers of tens or even hundreds of nanometer thickness, so that the quantum effects are reduced; nevertheless they are also called in some texts "quantum well" PV cells (see for instance Ref. 5). However, MLPV cells with real quantum sizes (multi-layered quantum well photovoltaic – MLQWPV) are also studied (e.g. in Refs. 14, 15).

The E 2456-06 ASTM International Standard "Terminology for Nanotechnology" states that sizes between 0.1 and 1 μm are to be called "submicronic", while the prefix "nano" is to be used for sizes between 1 and 100 nm only. On the other hand, an analysis of the quantum effects proves that the quantum size appears under about 20 interatomic distances (e.g. about 5 nm), where the band structure

---

[1]Faculty of Applied Sciences, University „Politehnica" of Bucharest, 313 Splaiul Independenţei Bucharest, 060042, Romania.

is replaced by an energy level structure and the momentum conservation law is no longer valid [16, 17].

The true quantum well photovoltaic cells use the special advantages of the low dimensional systems, where at least one size is at quantum scale. This leads to two important contributions.

• The first contribution is a strong quantum confinement (QC) effect. Indeed, at this size, it was proved that the material nature role is secondary with respect to the QC [18, 19].

• The second contribution is the increased role of the surface/interface. The area/volume ratio is of the order of $1/d$, where d is the minimum size, so that, at quantum sizes, this ratio is greater than 2×10^8 m^{-1}. Then, the cells are classified with respect to their dimensionality in 2D, 1D, 0D and fractals. The MLPV (and the multi-layered quantum well photovoltaic − MLQWPV) cells are 2D. In literature, they are divided in multiple quantum wells (MQW) and superlattice (SL) systems [5, 14], the difference being based on the barrier layer thickness [14]. However, this interpretation is not correct. The SL structures replace the resonant levels from the conduction and valence bands of the "quantum wells" with resonant bands. This is not correlated with the barrier thickness, but with the total number of layers, for reasons similar with those that define the quantum size [16, 17]. In the following, only MQW structures will be considered.

We have to mention the recent results obtained regarding plasmonic solar cells which have important prospects for the future. They use nanoparticles to benefit from plasmonic effect in order to improve absorption and finally, the solar cell current response [21].

The aim of this paper is to model MLQWPV cells in order to find out how to improve them. Section 2 deals with the QC effects. Section 3 calculates the quantum efficiency of a layer and discusses the optical improvements of the cells. Section 5 (the last) summarizes all the simulation results.

2. Quantum confinement effects

As we have stated in Section 1, the MLQWPV cells have a p-i-n structure, with a multi-layered i region (e.g. GaAs/Al$_x$Ga$_{1-x}$As). It is well known that the band gap difference between the layers acts like a quantum well and induces the appearance of resonant levels in both the conduction and valence bands (MQW structure). These levels improve the absorption and therefore increase the cell efficiency. If the number of layers is big enough, the resonant levels are replaced with resonant bands (SL structure). An example of both structures, under an external bias V, is presented in Fig. 1, adapted from Fig. 2 (see [12]). E_w, t_w and E_b, t_b are the gaps

and thicknesses of the quantum well and barrier layers, respectively. For MLQWPV cells, both t_w and t_b are of the order of $5 - 10$ nm.
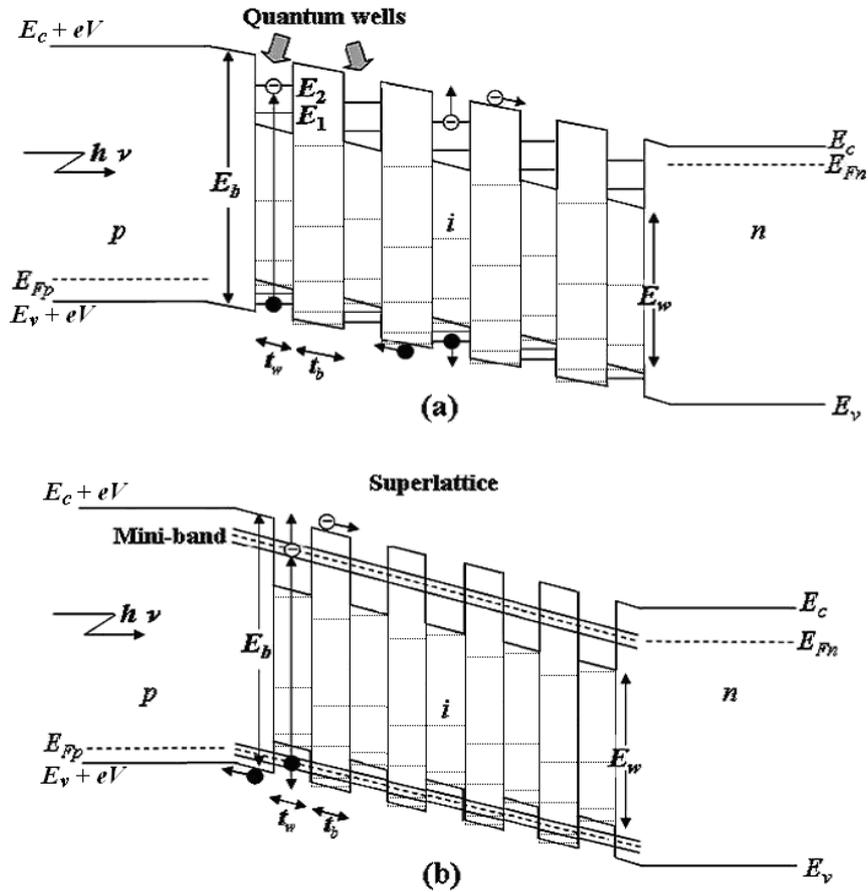
Fig. 1. (a) MQW and (b) SL p-i-n structures under applied bias V. Solid lines - the resonant levels (a) and bands (b); dotted lines - the QC levels.

Several studies [18-20] proved that the main quantum confinement (QC) effect consists in the introduction of QC levels in the band gap. Indeed, the surface/interface of a low dimensional system acts like the wall of a quantum well. The analysis of different shapes proved that the rectangular quantum well is good enough for the description of the QC effects.

There are two more problems to analyze.

   •   The first one is the depth of the potential well. We have found that, for rectangular quantum wells, deeper than 2 eV and larger than 1 nm, the differences between the first three levels in the finite well and the infinite well with the same width is less than 2.5 % [18], so that the use of the infinite rectangular quantum well (IRQW) approximation does not exceed the

experimental errors. As the relative error is proportional with $t\sqrt{U}$, where U is the potential well depth, it results that the IRQW approximation does not lead to errors greater than about 5 % for any known MQW or SL structure.

• The second problem is the location of these additional energy levels. As at absolute zero temperature the maximum energy of an electron in a semiconductor corresponds with the top of the valence band, the fundamental quantum confinement level should be located at this energy value. This means that the QC levels must be located in the band gap.

The electron energy has the expression:

$$E = \varepsilon_{n\vec{k}} + \frac{2\pi^2\hbar^2}{m_t^* t^2}p^2 = \left(\varepsilon_{n\vec{k}} + \frac{2\pi^2\hbar^2}{m_t^* t^2}\right) + \frac{2\pi^2\hbar^2}{m_t^* t^2}\left(p^2 - 1\right) \equiv \varepsilon_{n\vec{k}}^{(s)} + E_{p-1} \qquad (1)$$

where $\varepsilon_{n\vec{k}}^{(s)}$ is the shifted 2D band energy, E_{p-1} is the QC level energy ($E_0 \equiv 0$), m_t^* is the transversal effective electron mass, and t the layer thickness. These QC levels induce supplementary absorption in the visible and near infrared range. It is important to remark that these levels appear in both narrow and wide gap layers. At the same time, one can see from Fig. 1 that, at convenient bias value, some levels from the consecutive quantum well and barrier layers have practically the same energy value (differences under k_BT). This strongly increases the tunneling rate through the junction.

3. Internal quantum efficiency modeling

We will not discuss here the band-to-band absorption, but only the absorption induced by the resonant levels and by the QC levels from the gap. The absorption rate is proportional with the square modulus of the matrix element of the transition Hamiltonian between the initial and final state:

$$R_\lambda = \frac{2\pi}{\hbar}\left|H_{fi}\right|^2\delta\left(\Delta E - \frac{hc}{\lambda}\right) \qquad (2)$$

If one takes into account only the electric dipole transition (as it is the most probable) and if one uses the IRQW approximation, the matrix element becomes:

$$H_{fi} = -\frac{2}{t}e\int_0^t \vec{E}\cdot\vec{r}\sin\frac{p_f\pi z}{t}\sin\frac{p_i\pi z}{t}\,dz \qquad (3)$$

where p_i, p_f are natural non-zero numbers.

The calculations are performed for $\vec{E}$ parallel with or perpendicular on the layer, considering a square cell with the size L. In the first case, the position vector does not depend on z and its mean value is $L/2$. Then, the matrix element equals $eE_{x,y}L/2$ if and only if $p_f = p_i$. This case describes the pair generation by means of

transitions between resonant states from the valence and conduction bands. In the second case, the matrix element is $eE_{x,y}t/2$ if $p_f = p_i$ (transitions between resonant states) and

$$H_{fi} = \frac{eE_z t}{\pi^2}\left[\frac{1-(-1)^{n_f-n_i}}{(n_f-n_i)^2} - \frac{1-(-1)^{n_f+n_i}}{(n_f+n_i)^2}\right] \tag{4}$$

(transitions between QC levels), which is different from zero if and only if $p_f - p_i = 2p - 1$. Usually, the transitions between QC levels start from $p_i = 1$ (top of the valence band). Taking into account the Snell-Descartes rule, we can express E_z for different polarizations. For polarization parallel with the incidence plane, $E_{\|z} = E_\| \sin i / \sqrt{\varepsilon_r} = \sqrt{E_\|^2 - E_{\|x,y}^2}$ (i is the external incidence angle), while for polarization perpendicular on the incidence plane $E_{\perp z} = 0$. As the solar light is not polarized, $E_\| = E_\perp = E/\sqrt{2}$. Then, the absorption rate is

$$R_\lambda = \frac{\pi e^2 \langle E^2 \rangle}{\hbar}\left[L^2\left(1 - \frac{\sin^2 i}{4\varepsilon_{rw}}\right) + t_w^2 \frac{\sin^2 i}{4\varepsilon_{rw}}\right]\delta\left(\Delta E - \frac{hc}{\lambda}\right) \tag{5}$$

for transitions between resonant symmetric levels in the quantum well (ε_{wr} is the relative permittivity and $\Delta E = hc/\lambda = E_w + \pi^2\hbar^2/2m_w^* t_w^2$, where $m_w^* = (1/m_{ew}^* + 1/m_{gw}^*)^{-1}$ is the excitonic effective mass) and

$$R_{\lambda_p} = \frac{512 e^2 t_{w,b}^2 \langle E^2 \rangle}{\pi^3 \hbar \varepsilon_{rw,b}} \cdot \frac{p^2 \sin^2 i}{(4p^2-1)^4}\delta\left(\Delta E_p - \frac{hc}{\lambda_p}\right) \tag{6}$$

for transitions between the top of the valence band and the QC levels ($\Delta E_p = hc/\lambda_p = (\pi^2\hbar^2/2m_{ew,b}^* t_{w,b}^2)\cdot(4p^2-1)$ and the constants correspond to the considered layer – either quantum well or barrier).

The Einstein absorption coefficient for a layer becomes

$$B_\lambda = \frac{\pi e^2 L^2}{\hbar^2 \varepsilon_0 \varepsilon_{rw}}\left[\left(1 - \frac{\sin^2 i}{4\varepsilon_{rw}}\right) + \frac{t_w^2}{L^2}\frac{\sin^2 i}{4\varepsilon_{rw}}\right] \tag{7}$$

for transitions between resonant symmetric levels in the quantum well and

$$B_{\lambda_p} = \frac{512 e^2 L^2}{\pi^3 \hbar^2 \varepsilon_0 \varepsilon_{rw,b}^2} \cdot \frac{t_{w,b}^2}{L^2}\frac{p^2 \sin^2 i}{(4p^2-1)^4} \tag{8}$$

for transitions between the top of the valence band and the QC levels.

The quantum efficiency is related to the Einstein absorption coefficient by the relation

$$\eta = \frac{8\pi\hbar}{cL^2}B \tag{9}$$

so that we obtain

$$\eta_\lambda = \frac{8\pi^2 e^2}{c\hbar\varepsilon_0\varepsilon_{rw}}\left[\left(1 - \frac{\sin^2 i}{4\varepsilon_{rw}}\right) + \frac{t_w^2}{L^2}\frac{\sin^2 i}{4\varepsilon_{rw}}\right] \tag{10}$$

$$\eta_{\lambda_p} = \frac{4096 e^2}{\pi^2 c\hbar\varepsilon_0\varepsilon_{rw,b}^2}\cdot\frac{t_{w,b}^2}{L^2}\frac{p^2\sin^2 i}{\left(4p^2 - 1\right)^4} \tag{11}$$

One can observe that the quantum efficiency for the transitions between the top of the valence band and the QC levels is several orders of magnitude smaller than the one for transitions between resonant symmetric levels in the quantum well. However, the excitation of even a few carriers in the band gap, on QC levels that are practically equal between the different layers (due to a conveniently chosen bias), leads to a photoassisted tunneling and significantly increases the photocurrent.
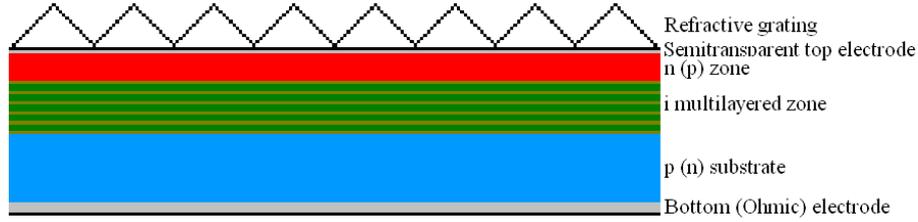
Fig. 2. Schematics of a p-i-n MLQWPV cell with refractive grating.

This condition could be assured if we would consider a refraction grating made up from optical prisms with the edges oriented on to the direction east-west (see figure 2). In this case, the following replacement could be done in the equations 10 and 11:

$$\sin^2 i \Rightarrow \sin^2 i + \cos^2\frac{\alpha}{2}\left(n_p^2 - 1 + 2\sin^2\frac{\alpha}{2}\cos^2 i - 2\sin\frac{\alpha}{2}\sqrt{n_p^2 - 1 + \sin^2\frac{\alpha}{2}\cos^2 i}\right) \tag{12}$$

where α is the prism angle and i is the incidence angle with the considered layer surface.

4. Simulation Results

4.1. Solar Cells Dimensions and Material Data

Based on the equations 10, 11 and 12 simulations have been carried out for cells with the dimension of 2.5 cm and the well thickness of 10 nm. The following values were considered for the general constants:

- electron mass $m_e = 9.1 \cdot 10^{-31}$ kg,
- Planck constant: $h = 6.6206 \cdot 10^{-34}$ J s,
- Speed of light : $c = 2.998 \cdot 10^8 \dfrac{m}{s}$,
- Vacuum absolute permittivity: $\varepsilon_0 = 8.854 \cdot 10^{-12} \dfrac{F}{m}$.

The analysed materials were GaAs and $Al_xGa_{1-x}As$.

$$\varepsilon_r = a_0 \left\{ f(\chi) + \frac{f(\chi_0)}{2} \left(\frac{e_0}{\delta_0} \right)^{\frac{3}{2}} \right\} + b_0 \tag{13}$$

$$a_0 = 6.3 + 19 \cdot x; \ b_0 = 9.4 - 10.2 \cdot x; \ f(\chi) = \frac{2 - \sqrt{1+\chi} - \sqrt{1-\chi}}{\chi^2}; \ \chi = \frac{hc}{e_0};$$

$$\chi_0 = \frac{hc}{\delta_0}; \ e_0 = 1.425 + 1.155 \cdot x + 0.37 \cdot x^2; \ \delta_0 = 1.765 + 1.115 \cdot x + 0.37 \cdot x^2.$$

Equation (13) is satisfied for $x \in [0, 1]$.

The material constants utilised for GaAs were:

- energy gap: $E_g = 1.424$ eV;
- effective mass of electron: $m_e^* = 0.067 \cdot m_e$;
- effective mass of gap: $m_g^* = 0.62 \cdot m_e$.

Material constants utilised for $Al_xGa_{1-x}As$

- effective mass of electron : $m_e^* = (0.067 + 0.083 \cdot x) \cdot m_e$.

4.2. Simulation of the Einstein absorption coefficients

Simulation of the Einstein absorption coefficients based on equations (7), (8) and (12) established in previous section the Einstein absorption coefficients were simulated as follows:

- Dependence of the Einstein absorption coefficient for the transitions between the resonant symmetric level in quantum well with the prism refraction index and incidence angle (see the figures 3 and 4).
- Dependence of the Einstein absorption coefficients for transitions between the top of the valence bands and the QC levels with the incidence angle and well thickness (see the figures 5 and 6).

The well thickness was $t_w = 10$ nm.
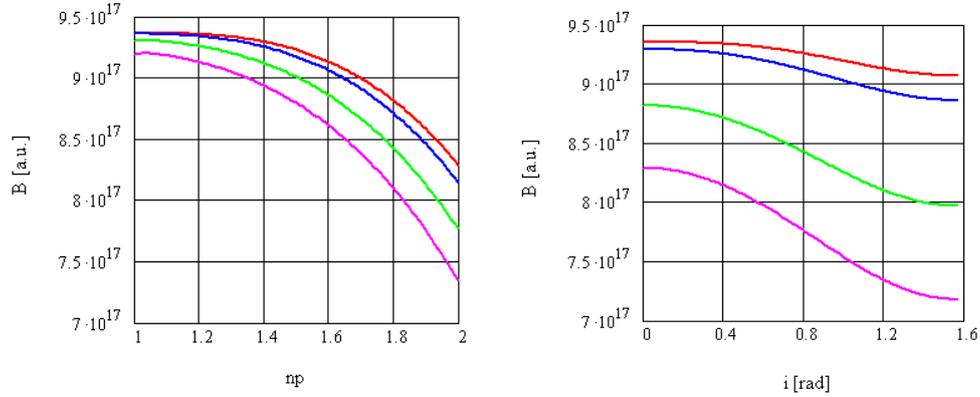
Fig. 3. (a) Dependence of the Einstein absorption coefficient for the transitions between the resonant symmetric level in quantum well on the prism refraction index. The following incidence angles were considered: i= 0 rad (red); i= 0.4 rad (blue); i= 0.8 rad (green); i=1.2 rad (violet); a.u. = atomic units.

(b) Dependence of the Einstein absorption coefficient for the transitions between the resonant symmetric level in quantum wells on the incidence angle. There were considered n_p=1.2 (red), n_p=1.4 (blue), n_p=1.8 (green), n_p=2 (violet).
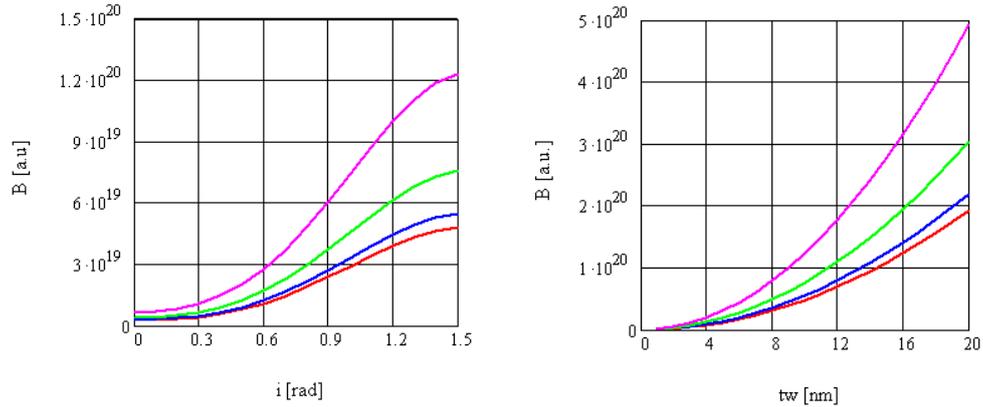
Fig. 4. (a) Dependence of the Einstein absorption coefficients for transitions between the top of the valence bands and the QC levels on incidence angle. There were considered different values for the aluminium amount x in the considered semiconductor: x= 0.1 (red); x= 0.2(blue); x= 0.4 (green); x=0.6 (violet).

(b) Dependence of the Einstein absorption coefficients for transitions between the top of the valence bands and the QC levels on well thickness (t_w). There were considered different for the aluminium amount in the considered semiconductor: x = 0.1 (red); x = 0.2 (blue); x = 0.4 (green); x = 0.6(violet).

4.3. Simulation of the quantum efficiency for the transitions between the resonant levels

The quantum efficiency of the transition between the resonant levels for GaAs was simulated based on the equations (10), (11) and (12).

The dependences on prism refraction index, as well as on incidence angle were studied (see figure 7 and 8).
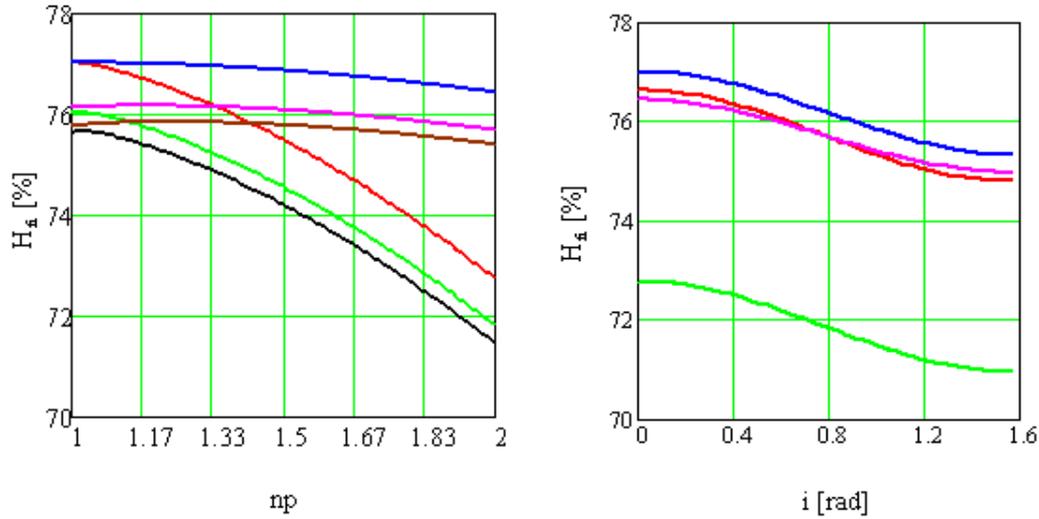
Fig. 5. (a)Quantum Efficiency of the transitions between the resonance level for GaAs as a function of prism refraction index. There were considered the following two main cases: (1) prism angle $\alpha = \pi/6$ and incidence angle: i=0 rad (red curve), i=0.8 rad (green curve), i=1 rad (black curve). (2) prism angle $\alpha = 2\pi/3$ and incidence angle: i=0 rad (blue curve), i=0.8 rad (violet curve), i=1 rad (brown).

(b) Quantum Efficiency of the transition between the resonant levels for GaAs as function of incidence angle.

From the Figures 6(a) and 6(b) it was remarked that the quantum efficiency of the transitions between the confinement levels has very small values in comparison with the quantum efficiency between the resonant levels.

It is smaller for larger prism angle α and it increases slowly together with the increasing of the incidence angle.

4.4. Simulation of the quantum efficiency for the transitions between the confinement levels

From the Figures 7(a) and 7(b) it was remarked that the quantum efficiency of the transitions between the confinement levels for $Al_xGa_{1-x}As$ the following features:

- it has larger values than for GaAs,

- it is increasing together with the increase of the aluminum amount as well as the refraction index of the prism,

- it is dropping with the increase of the incidence angle.
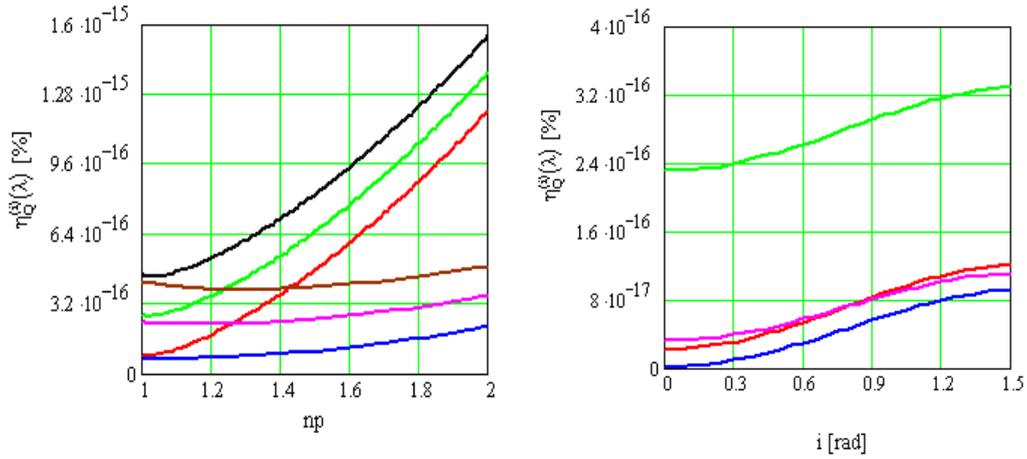
Fig. 6. (a) Quantum efficiency for the transitions between confinement levels for Al$_x$Ga$_{1-x}$As as functions of prism refraction index. There were considered two main cases: (1) prism angle $\alpha = \pi / 6$ and incidence angle: i=0.4 rad (red curve), i=0.8 rad (green curve) and i=1.2 (black curve) (2) prism angle $\alpha = 2\pi/3$ incidence angle i=0.4 rad (blue curve), i=0.8 rad (violet curve) and i=1.2 (brown curve).

(b) Quantum efficiency for the transitions between confinement levels for Al$_x$Ga$_{1-x}$As as function incidence angle. There were considered two main cases: (1) prism angle $\alpha = \pi / 6$ and prism refraction index: n$_p$=1.2 rad (red curve), n$_p$=2 rad (green curve) (2) prism angle $\alpha = 2\pi/3$ incidence angle n$_p$ =1.2 rad (blue curve), n$_p$ = 2 rad (violet curve).
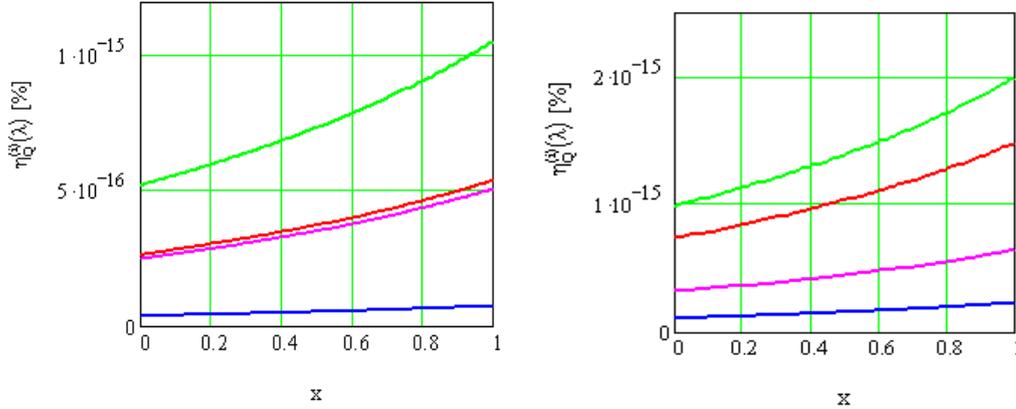
Fig. 7. (a) Quantum efficiency for the transitions between confinement levels for Al$_x$Ga$_{1-x}$As as function of aluminium amount. The prism refraction index is $n_p = 1.5$. There were considered two main cases: (1) prism angle $\alpha = \pi / 6$ and incidence angle: i=0.2 rad (red curve), i=1.2 rad (green curve) (2) prism angle $\alpha = 2\pi/3$ and incidence angle: i=0.2 rad (blue curve), i=1.2 rad (violet curve).

(b) Quantum efficiency for the transitions between confinement levels for Al$_x$Ga$_{1-x}$As as function of aluminum amount. The prism refraction index is n$_p$ = 2. There were considered two main cases: (1) prism angle $\alpha = \pi / 6$ and incidence angle: i=0.2 rad (red curve), i=1.2 rad (green curve) (2) prism angle $\alpha = 2\pi/3$ and incidence angle: i=0.2 rad (blue curve), i=1.2 rad (violet curve).

Conclusions

We have proved that the QC introduces energy levels not only in the conduction and valence bands (resonant levels), but also in the band gaps (QC levels). The corresponding energy values can be estimated from IRQW approximation with a good precision. On this basis, the quantum efficiency of the absorption for transitions between resonant or QC levels was calculated. A refractive grating was proposed in order to ensure good absorption conditions at any Sun position. Such an adaption could provide to the present MLQWPV cells several advantages over the classical PV cells: increased efficiency, wider spectral response, increased controllability. The simulated curves for the transition between the resonant levels as well as the transition between the confinement levels were presented and discussed.

The modelled and simulated results would allow an improved design of the quantum well solar cells.

Acknowledgment

R E F E R E N C E S

[1] K.W.J. Barnham and G. Duggan, A new approach to high-efficiency multi-band-gap solar cells, J. Appl. Phys. 67 (1990) 3490 - 3493.

[2] K.W.J. Barnham, B. Braun, J. Nelson, M. Paxman, Short-circuit current and energy efficiency enhancement in a low-dimensional structure photovoltaic device, Appl. Phys. Lett. 59 (1991) 135 - 137.

[3] M. Paxman, J. Nelson, B. Braun, J. Connolly, K. W. J. Barnham, C. T. Foxon, and J. S. Roberts, Modeling the spectral response of the quantum well solar cell, J. Appl. Phys. 74 (1993) 614 - 621.

[4] N. G. Anderson, Ideal theory of quantum well solar cells, J. Appl. Phys. 78 (1995) 1850 - 1861.

[5] J. P. Connolly, Modelling and optimising GaAs/AlxGa1-xAs multiple quantum well solar cells, Ph.D. Thesis, Department of Physics, Imperial College of Science, Technology and Medicine, University of London, UK, 1997.

[6] O. Y. Raisky, W. B. Wang, R. R. Alfano, C. L. Reynolds Jr., D. V. Stampone, and M. W. Focht, Resonant enhancement of the photocurrent in multiple-quantum-well photovoltaic devices, Appl. Phys. Lett. 74 (1999) 129-131.

[7] M. A. Green, Prospects for photovoltaic efficiency enhancement using low-dimensional structures, Nanotechnology 11 (2000) 401-405.

[8] K.W.J. Barnham, I. Ballard, J.P. Connolly, N.J. Ekins-Daukes, B.G. Kluftinger, J. Nelson, C. Rohr, Quantum well solar cells, Physica E 14 (2002) 27 - 36.

[9] N. G. Anderson, On quantum well solar cell efficiencies, Physica E 14 (2002) 126-131.

[10] P. Abbott, Characterisation of Quantum Well Solar Cells for Low Temperature Thermophotovoltaic Applications, Ph.D. Thesis, Department of Physics, Imperial College of Science, Technology and Medicine, University of London, UK, 2003.

[11] Y. Sato, K. Yamagishi, and M. Yamashita, Multilayer Structure Photovoltaic Cells, Opt. Rev. 12 (2005) 324 - 327.

[12] O. Jani, C. Honsberg, A. Asghar, D. Nicol, I. Ferguson, A. Doolittle, and S. Kurtz, Characterization and analysis of InGaN photovoltaic devices, in Proc. 31st IEEE Photovoltaic Specialists Conf., 3-7 Jan. 2005, Orlando, USA, 2005.

[13] A. G. Norman, M. C. Hanna, P. Dippo, D. H. Levi, R. C. Reedy, J. S. Ward, and M. M. Al-Jassim, InGaAs/GaAs QD superlattices: MOVPE growth, structural and optical characterization and application in intermediate-band solar cells, in Proc. 31st IEEE Photovoltaic Specialists Conf., 3-7 Jan. 2005, Orlando, USA, 2005.

[14] S. Y. Myong, Recent progress in inorganic solar cells using quantum structures, Recent Patents Nanotechnol. 1 (2007) 67-73.

[15] Z. R. Hong, B. Maennig, R. Lessmann, M. Pfeiffer, K. Leo, and P. Simon, Improved efficiency of zinc phthalocyanine/C60 based photovoltaic cells via nanoscale interface modification, Appl. Phys. Lett. 90 (2007) 230505–1-3.

[16] J. Heitmann, F. Müller, L. X. Yi, M. Zacharias, D. Kovalev, and F. Eichhorn, Excitons in Si nanocrystals: Confinement and migration effects, Phys. Rev. B 69 (2004) 195309.

[17] L. Fara, V. Iancu, M. R. Mitroi, and E, Nistor, Physical bases of the nanotechnologies, applications and perspectives (in Romanian), Punct, Bucharest, 2007 (in press).

[18] V. Iancu and M. L. Ciurea, Quantum confinement model for electric transport phenomena in fresh and stored photoluminescent porous silicon films, Solid State Electron. 42 (1998) 1893-1896.

[19] V. Iancu, M. L. Ciurea, and I. Stavarache, Quantum confinement modeling of electrical and optical processes in nanocrystalline silicon, J. Optoelectron. Adv. Mater. 8 (2006) 2156-2160.

[20] O. Pana, L. M. Giurgiu, Al. Darabont, V. Iancu, M. L. Ciurea, M. N. Grecu, Core-shell effects in granular perovskite manganites, J. Phys. Chem. Solids, 67 (2006) 624–627.

[21] K. R. Catchpole, A. Polman, "Plasmonic Solar Cells", Opt. Express, 16 (2008) 21793-21800.